Mesh U-Nets for 3D Cardiac Deformation Modeling

Marcel Beetz[1(✉)], Jorge Corral Acero[1], Abhirup Banerjee[1,2], Ingo Eitel[3,4,5], Ernesto Zacur[1], Torben Lange[6,7], Thomas Stiermaier[3,4,5], Ruben Evertz[6,7], Sören J. Backhaus[6,7], Holger Thiele[8,9], Alfonso Bueno-Orovio[10], Pablo Lamata[11], Andreas Schuster[6,7], and Vicente Grau[1]

[1] Department of Engineering Science, Institute of Biomedical Engineering, University of Oxford, Oxford, UK
marcel.beetz@eng.ox.ac.uk
[2] Division of Cardiovascular Medicine, Radcliffe Department of Medicine, University of Oxford, Oxford, UK
[3] University Heart Center Lübeck, Medical Clinic II, Cardiology, Angiology, and Intensive Care Medicine, Lübeck, Germany
[4] University Hospital Schleswig-Holstein, Lübeck, Germany
[5] German Centre for Cardiovascular Research, Partner Site Lübeck, Lübeck, Germany
[6] Department of Cardiology and Pneumology, University Medical Center Göttingen, Georg-August University, Göttingen, Germany
[7] German Centre for Cardiovascular Research, Partner Site Göttingen, Göttingen, Germany
[8] Department of Internal Medicine/Cardiology, Heart Center Leipzig at University of Leipzig, Leipzig, Germany
[9] Leipzig Heart Institute, Leipzig, Germany
[10] Department of Computer Science, University of Oxford, Oxford, UK
[11] Department of Biomedical Engineering, King's College London, London, UK

Abstract. During a cardiac cycle, the heart anatomy undergoes a series of complex 3D deformations, which can be analyzed to diagnose various cardiovascular pathologies including myocardial infarction. While volume-based metrics such as ejection fraction are commonly used in clinical practice to assess these deformations globally, they only provide limited information about localized changes in the 3D cardiac structures. The objective of this work is to develop a novel geometric deep learning approach to capture the mechanical deformation of complete 3D ventricular shapes, offering potential to discover new image-based biomarkers for cardiac disease diagnosis. To this end, we propose the *mesh U-Net*, which combines mesh-based convolution and pooling operations with U-Net-inspired skip connections in a hierarchical step-wise encoder-decoder architecture, in order to enable accurate and efficient learning directly on 3D anatomical meshes. The proposed network is trained to model both cardiac contraction and relaxation, that is, to predict the 3D cardiac anatomy at the end-systolic phase of the cardiac cycle based on the corresponding anatomy at end-diastole and vice versa. We evaluate our

O. Camara et al. (Eds.): STACOM 2022, LNCS 13593, pp. 245–257, 2022.
https://doi.org/10.1007/978-3-031-23443-9_23

method on a multi-center cardiac magnetic resonance imaging (MRI) dataset of 1021 patients with acute myocardial infarction. We find mean surface distances between the predicted and gold standard anatomical meshes close to the pixel resolution of the underlying images and high similarity in multiple commonly used clinical metrics for both prediction directions. In addition, we show that the mesh U-Net compares favorably to a 3D U-Net benchmark by using 66% fewer network parameters and drastically smaller data sizes, while at the same time improving predictive performance by 14%. We also observe that the mesh U-Net is able to capture subpopulation-specific differences in mechanical deformation patterns between patients with different myocardial infarction types and clinical outcomes.

Keywords: Geometric deep learning · 3D heart contraction · Cardiac mechanics · Acute myocardial infarction · Cardiac MRI · Spectral graph convolutions · Mesh sampling

1 Introduction

The human heart undergoes a series of complex 3D deformations during a normal heartbeat that are crucial for its correct operation. Accordingly, cardiac contraction and relaxation patterns are routinely analyzed in clinical practice to detect, diagnose, and treat a variety of cardiac diseases, including acute myocardial infarction. However, current clinical decision-making is usually based on relatively coarse global metrics of cardiac function, such as ejection fraction, that neglect more localized and intricate cardiac shape changes and therefore limit the clinical accuracy. Hence, many previous works have studied temporal deformations of the heart in a more holistic manner and in a variety of different settings using generative adversarial networks [24], graph neural networks [9,21–23], Siamese recurrent neural networks [26], principal component analysis [7], manifold learning [11], probabilistic encoder-decoder models [16], time-series autoencoders [5], point cloud autoencoders [1–4], or systems of differential equations [14,17,19].

However, these approaches are either limited to synthetic anatomy models with only a limited number of different cardiac shapes [9], lack validation on pathological datasets [4,21,22,24], use low-dimensional representations of the cardiac anatomy [5,21,22,24], consider cardiac contraction but not relaxation [21,22,24], use inefficient and memory-intensive voxelgrids to represent cardiac anatomical surfaces [16,26], or require special post-processing steps for common follow-up tasks due to a lack of explicit connectivity information in point clouds [1–4]. In this work, our aim is to develop a novel data-driven approach that is able to accurately capture and predict the complex deformations of pathological 3D cardiac shapes between the end-diastolic (ED) and the end-systolic (ES) phases of the cardiac cycle in an effective and efficient manner. To this end, we propose the *mesh U-Net*, a new geometric deep learning architecture, which combines

mesh-based convolution and pooling operations with the hierarchical encoder-decoder structure of the U-Net to enable the direct and effective processing of high-resolution 3D anatomical surface meshes. We find that the mesh U-Net can successfully model and differentiate complex cardiac mechanics patterns on an individual, subpopulation, as well as the whole-population level, allowing for improved understanding of different myocardial infarction (MI) types and more interpretable risk identification of major adverse cardiac events based on novel image-based biomarkers.

2 Methods

2.1 Dataset and Preprocessing

The dataset used in this work consists of cine MRI acquisitions from 1021 patients with MI. The MI event occurred at a median of 3 days prior to imaging and was classified as ST-elevation myocardial infarction (STEMI) or non-ST-elevation myocardial infarction (non-STEMI). After a 12-months post-infarct follow-up period, 74 patients suffered a major adverse cardiac event (MACE) defined as either reinfarction, new congestive heart failure, or all-cause death. All images were acquired as part of two multi-center studies with a mean pixel resolution of 1.36 mm (range: [1.16, 2.08] mm, SD: 0.21 mm). Both the studies and acquisition protocols have previously been described in greater detail in [12,29]. We select the short-axis slices at both the ED and ES phases of the cardiac cycle of each patient and reconstruct the corresponding 3D mesh representations of the left ventricular (LV) myocardial anatomy using the multi-step process outlined in [7,8,18]. We then create a mean template mesh by averaging each of the vertex coordinates across the dataset and represent the anatomy of each patient as its vertex-wise deformation with respect to this mean mesh for network training. Finally, we apply standardization to all vertex coordinate values of both the input and output meshes of the network.

2.2 Network Design

The architecture of the proposed mesh U-Net follows a symmetric encoder-decoder design with 3D meshes as both network inputs and outputs (Fig. 1).

The encoder consists of four hierarchical mesh down-sampling steps creating successively coarser representations of the input mesh with each lower network level, while the decoder employs four corresponding up-sampling operations for symmetric step-wise increases in mesh resolution. Spectral graph convolutions are then used at each of the four resolution levels to enable multi-scale feature learning in both local and global contexts across a variety of cardiac shapes. Similar to the original U-Net architecture [28], we increase the number of feature maps of the graph convolution operations at deeper network levels as the mesh resolution decreases to facilitate the learning of more complex features. We also incorporate skip connections between the corresponding levels of the encoder

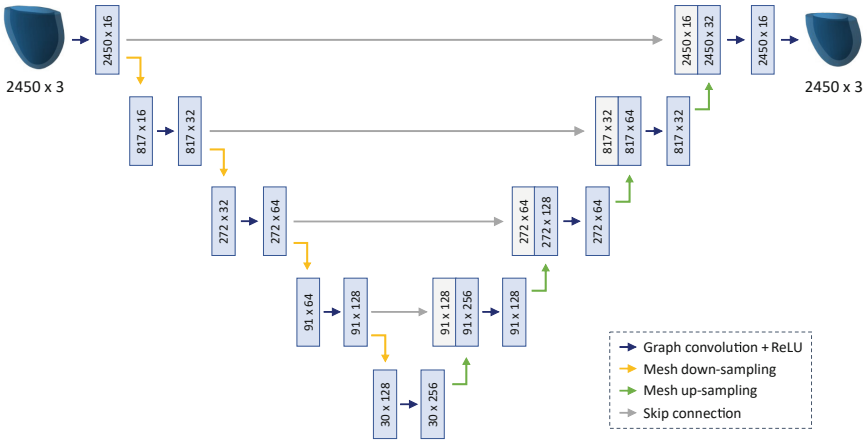

Fig. 1. Network architecture of the proposed mesh U-Net. A symmetric encoder-decoder structure with hierarchical mesh sampling operations and spectral graph convolutions enables efficient multi-scale feature learning directly on mesh data. U-Net inspired skip connections facilitate information flow between the encoder and decoder branches, while the number of feature maps steadily increases in lower network levels to capture more complex patterns. Surface meshes with 2450 vertices are used as network inputs and outputs to represent the cardiac anatomy at either ED or ES.

and decoder branches to allow for efficient information flow between earlier and later layers of the network. Both down-sampling and up-sampling layers are implemented using the quadric error minimization criterion [27] with three-fold reductions and increases in mesh resolution respectively at each network level. All graph convolutions utilize the Chebyshev polynomial approximation [10,13] of order 5 and are followed by rectified linear units (ReLU) as activation functions.

2.3 Implementation and Training

The deep learning code base is implemented using the PyTorch [25] framework. We train our models using the Adam optimizer [15] with a learning rate of 0.007, a batch size of 16, and a weight decay of 0.0006 for 250 epochs on a CPU with 8 GB memory. We select the L1 distance between the corresponding vertices in the predicted and gold standard meshes as our loss function and use a random train/validation/test dataset split of 80%/5%/15% for the prediction experiments in Sect. 3.1 and 3.2. The test dataset size in the subpopulation-specific experiments (Sect. 3.3) is set to the same number as the respective left-out subpopulation (i.e. n = 305 for STEMI/non-STEMI; n = 74 for non-MACE/MACE), while the remaining data is split into 95% training and 5% validation data. In all experiments, we select the model weights of the training checkpoint with the best performance on the validation dataset as our final model for evaluation on the test dataset.

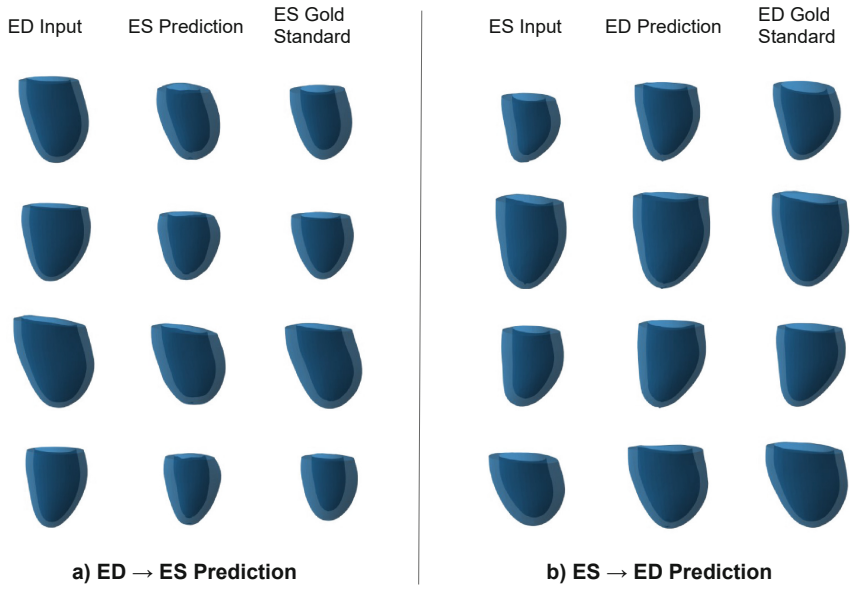

Fig. 2. ES prediction (a) and ED prediction (b) results of the mesh U-Net for four sample patients (in rows) of the unseen test dataset.

3 Experiments and Results

3.1 Prediction Quality

We first want to assess the mesh U-Net's ability to correctly predict cardiac shapes at ES from ED inputs and vice versa. To this end, we train two separate networks, one for each prediction direction, to analyze both cardiac contraction and relaxation. We then pass the input ED/ES cardiac meshes from the unseen test dataset through the pertinent trained network and compare the prediction outputs with the corresponding test dataset meshes at ES/ED, which we assume to be our gold standard. The qualitative results for four sample cases are displayed in Fig. 2-a and Fig. 2-b for the ES and ED prediction tasks, respectively.

We observe a good alignment between the predicted and gold standard meshes on both a local and global level and for a variety of different shapes, in both the ED and ES prediction tasks.

Next, we quantify the mesh U-Net's prediction performance by calculating both the mean surface distance (MSD) (Eq. 1) and the Hausdorff distance between each predicted mesh X and their corresponding gold standard mesh Y of the test dataset.

$$MSD(X,Y) = \frac{1}{2}\left(\frac{1}{|X|}\sum_{x\in X} d(x,Y) + \frac{1}{|Y|}\sum_{y\in Y} d(y,X)\right) \tag{1}$$

We select the 3D U-Net [6], whose voxelgrid-based design components have been widely utilized in previous works for 3D medical image processing and anatomical surface modelling, as a benchmark to evaluate our method and report the distance values obtained by both approaches and in both prediction tasks in Table 1. Further details on the training procedure of the 3D U-Net are provided in the Appendix.

Table 1. Quantitative prediction results of the mesh U-Net and 3D U-Net.

Input phase	Output phase	Method	Hausdorff distance (mm)	Surface distance (mm)
ED	ES	3D U-Net	8.02 (±3.26)	1.85 (±0.62)
		Mesh U-Net	7.06 (±2.31)	1.69 (±0.57)
ES	ED	3D U-Net	7.94 (±3.74)	1.78 (±0.81)
		Mesh U-Net	6.27 (±1.85)	1.44 (±0.39)

Values represent mean (± standard deviation (SD)).

We find that the mesh U-Net outperforms the 3D U-Net for both metrics and in both prediction directions, with mean surface distances similar to the pixel resolution of the underlying image acquisitions.

In addition to the prediction accuracy, we also compare the mesh U-Net and 3D U-Net architectures in terms of their data formats and number of network parameters (Table 2).

Table 2. Technical comparison of mesh U-Net and 3D U-Net.

Method	Data type	Data instance size	Network parameters
3D U-Net	Voxelgrid	$\sim 2.1 \times 10^6$ (128×128×128)	$\sim 2.0 \times 10^6$
Mesh U-Net	Mesh	$\sim 7.4 \times 10^3$ (2450×3)*	$\sim 6.8 \times 10^5$

*Vertex connectivity is the same for each mesh in the dataset.

We observe that the mesh U-Net only needs about 34% as many parameters as the 3D U-Net, while its usage of meshes to represent anatomical surface data allows for a drastic reduction in the required data sizes.

3.2 Clinical Evaluation

Next, we evaluate the mesh U-Net's ability to accurately capture the mechanical deformation of the heart from a clinical perspective. To this end, we first obtain the ES/ED predictions for all ED/ES input meshes of the test dataset from the respective networks. Then, we use these predicted mesh populations as well as the corresponding test set mesh populations, which we consider as our gold standard, to calculate multiple image-based biomarkers commonly used in clinical practice. We consider both cardiac anatomy metrics focusing on the heart at either ED or

Table 3. Clinical anatomy and function metrics results achieved by the mesh U-Net.

Input phase	Predicted phase	Clinical metric	Gold standard	Prediction
ED	ES	LV ES volume (ml)	80 (±31)	78 (±27)
		LV myocardial mass (g)	121 (±33)	120 (±27)
		LV stroke volume (ml)	68 (±21)	71 (±18)
		LV ejection fraction (%)	47 (±11)	47 (±14)
ES	ED	LV ED volume (ml)	148 (±37)	149 (±36)
		LV myocardial mass (g)	113 (±29)	115 (±24)
		LV stroke volume (ml)	73 (±22)	74 (±18)
		LV ejection fraction (%)	50 (±12)	51 (±11)

Values represent mean (± SD) in all cases.

ES (LV volume, LV mass) and cardiac function metrics which assess the temporal changes between cardiac shapes at ED and at ES (LV stroke volume, LV ejection fraction). The results for both prediction directions are reported in Table 3.

We find highly similar mean and standard deviation values between the gold standard and predicted mesh populations across both cardiac anatomy and function metrics and for both prediction directions.

3.3 Subpopulation-Specific Deformations

In addition to predicting mechanical shape changes for the whole population in the dataset, we also want to investigate whether the mesh U-Net can learn 3D deformation patterns that are specific to certain subpopulations. To this end, we first partition the original dataset into two subpopulations based on STEMI vs non-STEMI and also separately for non-MACE vs MACE. We then train a mesh U-Net on the data from one subpopulation (STEMI and non-MACE respectively) and evaluate its performance on both the unseen test dataset from the same subpopulation, as well as the meshes from the other subpopulation (non-STEMI and MACE respectively) that are not used during training. In this way, we are able to analyze possible differences in the distributions of surface distance values for both the matching and non-matching test datasets. We show the results for both outcomes and for both prediction directions in Fig. 3.

We find statistically significant differences in terms of Kolmogorov-Smirnov (KS) test ($p<0.005$ in all experiments) between the matching and non-matching performance distributions in all four experiments, with lower prediction errors for the matching datasets. This indicates that the mesh U-Net has learnt subpopulation-specific patterns, which cause the performance to deteriorate when applying the network to the other subpopulation whose unique patterns were not seen during training. While the findings displayed in Fig. 3 are based on surface distances, we observe similar results using Hausdorff distances as the comparative metric, which can be found in the Appendix.

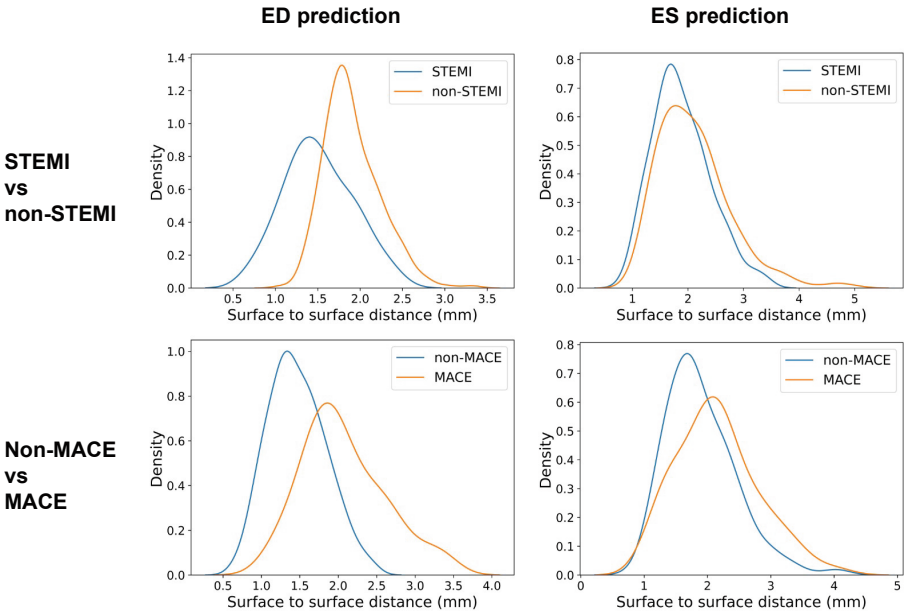

Fig. 3. Surface distance distributions achieved by mesh U-Nets trained on one subpopulation and evaluated on unseen test dataset of the same subpopulation (blue color) and the complementary subpopulation (orange color). Plots are shown for both ED and ES prediction tasks (columns) and both STEMI and MACE population splits (rows). p-values for KS-test: <0.0001 (ED prediction for both STEMI and MACE); <0.001 (ES prediction for MACE); <0.005 (ES prediction for STEMI). (Color figure online)

4 Discussion and Conclusion

In this work, we have presented the mesh U-Net, a novel geometric deep learning method, for efficient deformation modelling of 3D cardiac anatomy shapes. Its architecture relies on recent advances in mesh-specific convolution and pooling operations, giving it the ability to directly and effectively process anatomical surface mesh data and capture important features at multiple different scales in a hierarchical manner. Similar to the original U-Net architecture, skip connections enable an easy information exchange across different parts of the network, while the step-wise sampling operations along the symmetric encoder and decoder branches allow for smooth transitions between different scales. The mesh U-Net outperforms a 3D U-Net benchmark by a considerable margin in both the ED and ES prediction tasks, showing the high efficacy of the chosen architectural design in different bitemporal settings. The results are consistent across both the surface distance and Hausdorff distance metrics, demonstrating the high average

prediction accuracy as well as an improved robustness to outliers and artifacts. We also visually observe the good alignment between the predicted and gold standard cardiac shapes on both a local and global level further confirming its good performance. Prediction errors are generally the largest at the apical and basal areas of the heart, which we suspect to be at least partially caused by the limited amount of spatial information available in those areas in the original MRI acquisition and the 3D reconstruction process.

The mesh U-Net achieves high prediction accuracy with 66% fewer parameters than the 3D U-Net, while using meshes to store the same anatomical surface information with 99.6% smaller data instance sizes than the corresponding voxelgrid representations. This shows the high efficiency of the design, enabling easy training on a CPU instead of a GPU and the usage of fewer memory resources with higher resolution meshes without being limited by any voxel resolution, as is the case for voxelgrids. Furthermore, the mesh U-Net's predictions obtain highly realistic values in both cardiac anatomy and function metrics for both prediction directions with typical morphological differences between the ED and ES phases (e.g. thicker myocardium at ES, larger heart size at ED) correctly captured. This provides further evidence of a good population-wide performance from a clinical perspective and indicates that accurate deformation patterns in line with clinical practice are captured by the network for both cardiac contraction and relaxation. This is important for the accuracy of any computer-based model as well as its clinical acceptance. While we did not explicitly include any mechanical properties or patient metadata in this study, we hypothesize that the network was able to implicitly learn many pertinent features from the large population of heart shapes in order to still achieve the observed good prediction accuracy.

Finally, we find that the mesh U-Net is capable of learning deformation patterns specific to different pathological subpopulations. This shows that diseases affect the mechanical deformation of the heart in different ways, and allows for a better understanding and potential stratification of myocardial infarction types (such as STEMI and non-STEMI) based on differences between the predicted and true 3D shapes. The results are also plausible from a biomechanical perspective as mechanical properties within the left ventricular tissue are typically shared by patients with similar pathophysiological conditions and differ between patients with separate pathologies. In addition, the non-MACE vs MACE comparison demonstrates that deviations in prediction, which represents "healthy" cardiac function, against actual function measured from images can help identify subjects at risk. This approach is also highly interpretable, as its usage of high-resolution 3D meshes for both predicted and true cardiac anatomies allows an easy visualization of global and local differences between actually observed and expected healthy hearts, which is crucial for an application in clinical practice and the discovery of novel image-based biomarkers.

Acknowledgments. The authors express no conflict of interest. The work of MB is supported by the Stiftung der Deutschen Wirtschaft (Foundation of German Business). AB is a Royal Society University Research Fellow and is supported by the Royal Society (Grant No. URF\R1\221314). The work of AB and VG is supported by the British Heart Foundation (BHF) Project under Grant PG/20/21/35082. The work of VG is supported by the CompBioMed 2 Centre of Excellence in Computational Biomedicine (European Commission Horizon 2020 research and innovation programme, grant agreement No. 823712). The work of JCA is supported by the EU's Horizon 2020 research and innovation program under the Marie Sklodowska-Curie (g.a. 764738) and the EPSRC Impact Acceleration Account (D4D00010 DF48.01), funded by UK Research and Innovation. ABO holds a BHF Intermediate Basic Science Research Fellowship (FS/17/22/32644). The work is also supported by the German Center for Cardiovascular Research, the British Heart Foundation (PG/16/75/32383), and the Wellcome Trust (209450/Z/17).

A 3D U-Net

In this section, we describe in greater detail the training and validation procedure of the 3D U-Net [6] used for both the end-diastolic and end-systolic prediction tasks. First, we convert the mesh representations of the cardiac anatomies of the whole dataset into voxelgrids to allow for the same dataset to be used for both the 3D U-Net and mesh U-Net evaluation. We achieve this by voxelizing the 3D meshes and placing them in the center of $128 \times 128 \times 128$ voxelgrids where each voxel is encoded as either background (value: "0") or left ventricular myocardium (value: "1"). We then select a 3D U-Net architecture and train it using binary cross entropy as a loss function. Next, we pass the unseen test data through the trained 3D U-Net and convert the resulting predictions and corresponding gold standard anatomies from voxelgrid to 3D surface mesh representations with the marching cubes algorithm [20]. Finally, we use the obtained mesh representations to calculate both surface distances and Hausdorff distances between the meshes predicted by the 3D U-Net and the respective gold standard meshes.

B Subpopulation-Specific Deformations

We display the results of the subpopulation-specific training experiments using the Hausdorff distance as a quantitative metric in Fig. 4.

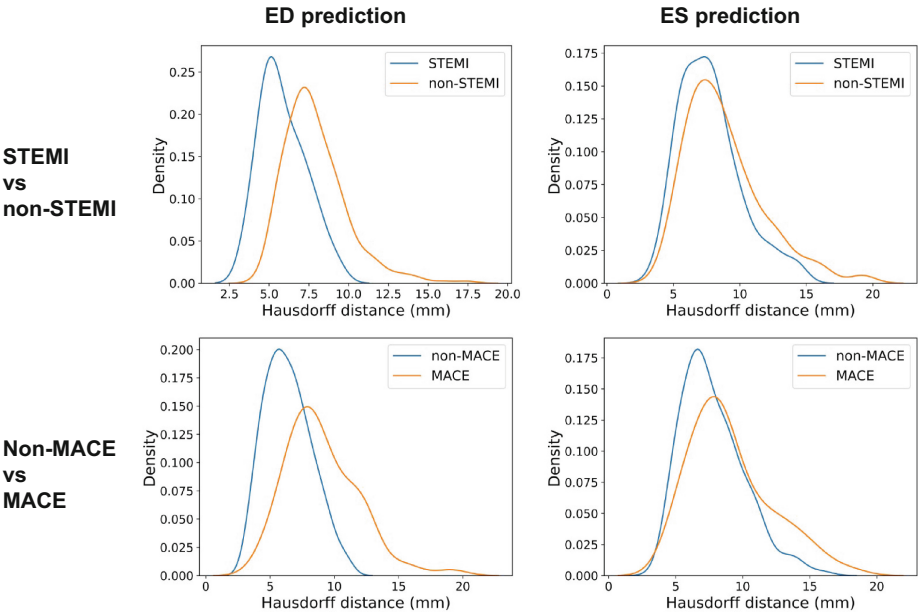

Fig. 4. Hausdorff distance distributions achieved by mesh U-Nets trained on one subpopulation and evaluated on unseen test dataset of the same subpopulation (blue color) and the complementary subpopulation (orange color). Plots are shown for both ED and ES prediction tasks (columns) and both STEMI and MACE population splits (rows). p-values for KS-test: <0.0001 (ED prediction for both STEMI and MACE); <0.001 (ES prediction for STEMI); <0.005 (ES prediction for MACE). (Color figure online)

References

1. Beetz, M., Banerjee, A., Grau, V.: Generating subpopulation-specific biventricular anatomy models using conditional point cloud variational autoencoders. In: Puyol Antón, E., et al. (eds.) STACOM 2021. LNCS, vol. 13131, pp. 75–83. Springer, Cham (2022). https://doi.org/10.1007/978-3-030-93722-5_9
2. Beetz, M., Banerjee, A., Grau, V.: Multi-domain variational autoencoders for combined modeling of MRI-based biventricular anatomy and ECG-based cardiac electrophysiology. Front. Physiol., 991 (2022)
3. Beetz, M., Banerjee, A., Sang, Y., Grau, V.: Combined generation of electrocardiogram and cardiac anatomy models using multi-modal variational autoencoders. In: 2022 IEEE 19th International Symposium on Biomedical Imaging (ISBI), pp. 1–4 (2022)
4. Beetz, M., Ossenberg-Engels, J., Banerjee, A., Grau, V.: Predicting 3D cardiac deformations with point cloud autoencoders. In: Puyol Antón, E., et al. (eds.) STACOM 2021. LNCS, vol. 13131, pp. 219–228. Springer, Cham (2022). https://doi.org/10.1007/978-3-030-93722-5_24
5. Bello, G.A., et al.: Deep-learning cardiac motion analysis for human survival prediction. Nat. Mach. Intell. **1**(2), 95–104 (2019)

6. Çiçek, Ö., Abdulkadir, A., Lienkamp, S.S., Brox, T., Ronneberger, O.: 3D U-Net: learning dense volumetric segmentation from sparse annotation. In: Ourselin, S., Joskowicz, L., Sabuncu, M.R., Unal, G., Wells, W. (eds.) MICCAI 2016. LNCS, vol. 9901, pp. 424–432. Springer, Cham (2016). https://doi.org/10.1007/978-3-319-46723-8_49
7. Corral Acero, J., et al.: Understanding and improving risk assessment after myocardial infarction using automated left ventricular shape analysis. JACC: Cardiovasc. Imaging (2022)
8. Corral Acero, J., et al.: SMOD - data augmentation based on statistical models of deformation to enhance segmentation in 2D cine cardiac MRI. In: Coudière, Y., Ozenne, V., Vigmond, E., Zemzemi, N. (eds.) FIMH 2019. LNCS, vol. 11504, pp. 361–369. Springer, Cham (2019). https://doi.org/10.1007/978-3-030-21949-9_39
9. Dalton, D., Lazarus, A., Rabbani, A., Gao, H., Husmeier, D.: Graph neural network emulation of cardiac mechanics. In: Proceedings of the 3rd International Conference on Statistics: Theory and Applications (ICSTA 2021), pp. 127-1-8 (2021)
10. Defferrard, M., Bresson, X., Vandergheynst, P.: Convolutional neural networks on graphs with fast localized spectral filtering. In: Proceedings of the 30th International Conference on Neural Information Processing Systems, pp. 3844–3852 (2016)
11. Di Folco, M., Moceri, P., Clarysse, P., Duchateau, N.: Characterizing interactions between cardiac shape and deformation by non-linear manifold learning. Med. Image Anal. **75**, 102278 (2022)
12. Eitel, I., et al.: Intracoronary compared with intravenous bolus abciximab application during primary percutaneous coronary intervention in ST-segment elevation myocardial infarction: cardiac magnetic resonance substudy of the AIDA STEMI trial. J. Am. Coll. Cardiol. **61**(13), 1447–1454 (2013)
13. Hammond, D.K., Vandergheynst, P., Gribonval, R.: Wavelets on graphs via spectral graph theory. Appl. Comput. Harm. Anal. **30**(2), 129–150 (2011)
14. Hong, B.D., Moulton, M.J., Secomb, T.W.: Modeling left ventricular dynamics with characteristic deformation modes. Biomech. Model. Mechanobiol. **18**(6), 1683–1696 (2019). https://doi.org/10.1007/s10237-019-01168-8
15. Kingma, D.P., Ba, J.: Adam: a method for stochastic optimization. arXiv preprint arXiv:1412.6980 (2014)
16. Krebs, J., Mansi, T., Ayache, N., Delingette, H.: Probabilistic motion modeling from medical image sequences: application to cardiac cine-MRI. In: Pop, M., et al. (eds.) STACOM 2019. LNCS, vol. 12009, pp. 176–185. Springer, Cham (2020). https://doi.org/10.1007/978-3-030-39074-7_19
17. Krishnamurthy, A., et al.: Patient-specific models of cardiac biomechanics. J. Comput. Phys. **244**, 4–21 (2013)
18. Lamata, P., et al.: An automatic service for the personalization of ventricular cardiac meshes. J. Roy. Soc. Interface **11**(91), 20131023 (2014)
19. Lopez-Perez, A., Sebastian, R., Ferrero, J.M.: Three-dimensional cardiac computational modelling: methods, features and applications. Biomed. Eng. Online **14**(1), 1–31 (2015)
20. Lorensen, W.E., Cline, H.E.: Marching cubes: a high resolution 3D surface construction algorithm. ACM SIGGRAPH Comput. Graph. **21**(4), 163–169 (1987)
21. Lu, P., Bai, W., Rueckert, D., Noble, J.A.: Modelling cardiac motion via spatio-temporal graph convolutional networks to boost the diagnosis of heart conditions. In: Puyol Anton, E., et al. (eds.) STACOM 2020. LNCS, vol. 12592, pp. 56–65. Springer, Cham (2021). https://doi.org/10.1007/978-3-030-68107-4_6

22. Lu, P., Bai, W., Rueckert, D., Noble, J.A.: Multiscale graph convolutional networks for cardiac motion analysis. In: Ennis, D.B., Perotti, L.E., Wang, V.Y. (eds.) FIMH 2021. LNCS, vol. 12738, pp. 264–272. Springer, Cham (2021). https://doi.org/10.1007/978-3-030-78710-3_26
23. Meister, F., et al.: Graph convolutional regression of cardiac depolarization from sparse endocardial maps. In: Puyol Anton, E., et al. (eds.) STACOM 2020. LNCS, vol. 12592, pp. 23–34. Springer, Cham (2021). https://doi.org/10.1007/978-3-030-68107-4_3
24. Ossenberg-Engels, J., Grau, V.: Conditional generative adversarial networks for the prediction of cardiac contraction from individual frames. In: International Workshop on Statistical Atlases and Computational Models of the Heart, pp. 109–118 (2019)
25. Paszke, A., et al.: PyTorch: an imperative style, high-performance deep learning library. In: Proceedings of the 33rd International Conference on Neural Information Processing Systems, pp. 8026–8037 (2019)
26. Qin, C., et al.: Joint learning of motion estimation and segmentation for cardiac MR image sequences. In: Frangi, A.F., Schnabel, J.A., Davatzikos, C., Alberola-López, C., Fichtinger, G. (eds.) MICCAI 2018. LNCS, vol. 11071, pp. 472–480. Springer, Cham (2018). https://doi.org/10.1007/978-3-030-00934-2_53
27. Ranjan, A., Bolkart, T., Sanyal, S., Black, M.J.: Generating 3D faces using convolutional mesh autoencoders. In: Proceedings of the European Conference on Computer Vision (ECCV), pp. 704–720 (2018)
28. Ronneberger, O., Fischer, P., Brox, T.: U-Net: convolutional networks for biomedical image segmentation. In: Navab, N., Hornegger, J., Wells, W.M., Frangi, A.F. (eds.) MICCAI 2015. LNCS, vol. 9351, pp. 234–241. Springer, Cham (2015). https://doi.org/10.1007/978-3-319-24574-4_28
29. Thiele, H., et al.: Effect of aspiration thrombectomy on microvascular obstruction in NSTEMI patients: the TATORT-NSTEMI trial. J. Am. Coll. Cardiol. **64**(11), 1117–1124 (2014)